Carrier-mediated nonlocal ferromagnetic coupling between local magnetic polarons in Fe-doped In_2O_3 and Co-doped ZnO

Shifei Qi,[1] Fengxian Jiang,[1] Jiuping Fan,[1] H. Wu,[1] S. B. Zhang,[2] Gillian A. Gehring,[3] Zhenyu Zhang,[4,5] and Xiaohong Xu[1,*]

[1]*School of Chemistry and Materials Science, Shanxi Normal University, Linfen 041004, People's Republic of China*

[2]*Department of Physics, Applied Physics, and Astronomy, Rensselaer Polytechnic Institute, Troy, New York 12180-3590, USA*

[3]*Department of Physics, University of Sheffield, Sheffield S3 7RH, United Kingdom*

[4]*ICQD/HFNL, University of Science and Technology of China, Hefei, Anhui 230026, People's Republic of China*

[5]*Department of Physics and Astronomy, University of Tennessee, Knoxville, Tennessee 37996, USA*

(Received 8 March 2011; revised manuscript received 15 August 2011; published 9 November 2011)

The combined roles of oxygen vacancy and electron doping in mediating local and nonlocal magnetic ordering of Fe doped in In_2O_3 and Co doped in ZnO have been investigated within first-principles density functional theory. We first show theoretically that two magnetic dopants can be stabilized energetically around an oxygen vacancy, and are ferromagnetically coupled to form a local magnetic polaron. Furthermore, electron doping plays the elegant dual role of further enhancing the ferromagnetic stability of a local polaron, and more crucially, mediating the nonlocal magnetic coupling between two polarons. Finally, we provide experimental evidence supporting these strong predictions.

DOI: 10.1103/PhysRevB.84.205204 PACS number(s): 75.50.Pp, 71.55.Eq, 85.30.De

I. INTRODUCTION

Diluted magnetic semiconductors (DMSs) have been actively studied as promising materials for developing spintronic devices.[1–4] However, transition-metal (TM) doped DMSs based on III-V (e.g., GaAs)[5] and IV (Ge or Si)[6] semiconductors generally possess relatively low Curie temperature (substantially lower than room temperature), which remains one of the main obstacles for device applications.

Since ZnO-based DMSs were predicted to exhibit high-temperature ferromagnetism,[1] a considerable number of studies of oxide-based DMSs have been made, often reporting room-temperature ferromagnetism or above.[7–11] Commonly invoked host materials include ZnO, TiO_2, In_2O_3, and SnO_2. Despite the progress in developing oxide DMSs, the underlying mechanism for ferromagnetic ordering is still under active debate. Competing mechanisms proposed include carrier-mediated exchange,[11] double exchange,[12] Zener model,[1] Ruderman-Kittel-Kasuya-Yoshida,[13] spin-split impurity band,[14] and bound magnetic polaron (BMP).[15] In these mechanisms, attention has been focused on mediating the ferromagnetic coupling between the magnetic dopants. More recently, a charge-transfer ferromagnetism (CTF) model has also been proposed to explain ferromagnetism in oxide DMSs.[16]

In the carrier-mediated model, the local moments on the TM dopants are coupled with each other ferromagnetically through polarized mobile carriers.[11] In the BMP model, the local moments on the TM dopants are coupled with each other ferromagnetically through polarized carriers trapped by defects, such as the electrons associated with an oxygen vacancy.[15] These models predict moments contributed by both the TM ions and the mediating polarized carriers (mobile or localized). In contrast, the CTF model predicts that the moments are entirely localized on itinerant carriers confined to small regions, possibly grain boundaries.[16] Although each model has its merits in certain aspects,[17–26] a complete understanding of the ferromagnetic behavior in oxide DMSs still calls for more microscopic insight into the defect structure, transport property, and moment distribution in these systems.

In this paper, we carry out comparative studies of two prototype systems, ZnO doped with Co or codoped with Co/Al, and In_2O_3 doped with Fe or codoped with Fe/Sn, to explore the roles of oxygen vacancy and electron doping in mediating the magnetic ordering in these systems using first-principles calculations. We find that, when two substitutional magnetic dopants are separated by an oxygen vacancy, ferromagnetic ordering is clearly favored. Such a configurational entity can be described as a BMP as proposed earlier,[15] whose validity is established here with first-principles accuracy. In addition, we find that electron doping not only can further enhance the ferromagnetic stability of the BMP, but more crucially, it mediates the nonlocal magnetic coupling between two BMPs. We also present preliminary experimental results supporting these predictions. We show that samples lose their magnetism after the number of oxygen vacancies is reduced by annealing in air, and this occurs even when the samples still show metallic conductivity due to ionized donors. This is in contrast with earlier studies in which both the magnetism and the metallic conductivity vanished after annealing in air.[27,28] These findings help to enrich our understanding of the microscopic origin of ferromagnetism in oxide DMSs.

II. METHOD AND COMPUTATIONAL DETAILS

The first-principles calculations were performed within the framework of density functional theory (DFT) and using the projector-augmented wave (PAW)[29] method as implemented in the VASP code.[30] We adopted the generalized gradient approximation (GGA) for treating the exchange-correlation interaction. The atomic geometries were fully optimized until the Hellmann-Feynman forces on each ion were <0.02 eV/Å. A plane-wave energy cutoff of 500 eV, a $3 \times 3 \times 3$ k-point grid, and the Gaussian smearing method with a 0.1 eV smearing width were used for the lattice relaxations. A $4 \times 4 \times 4$ k-point grid and the tetrahedron method were adopted in the final

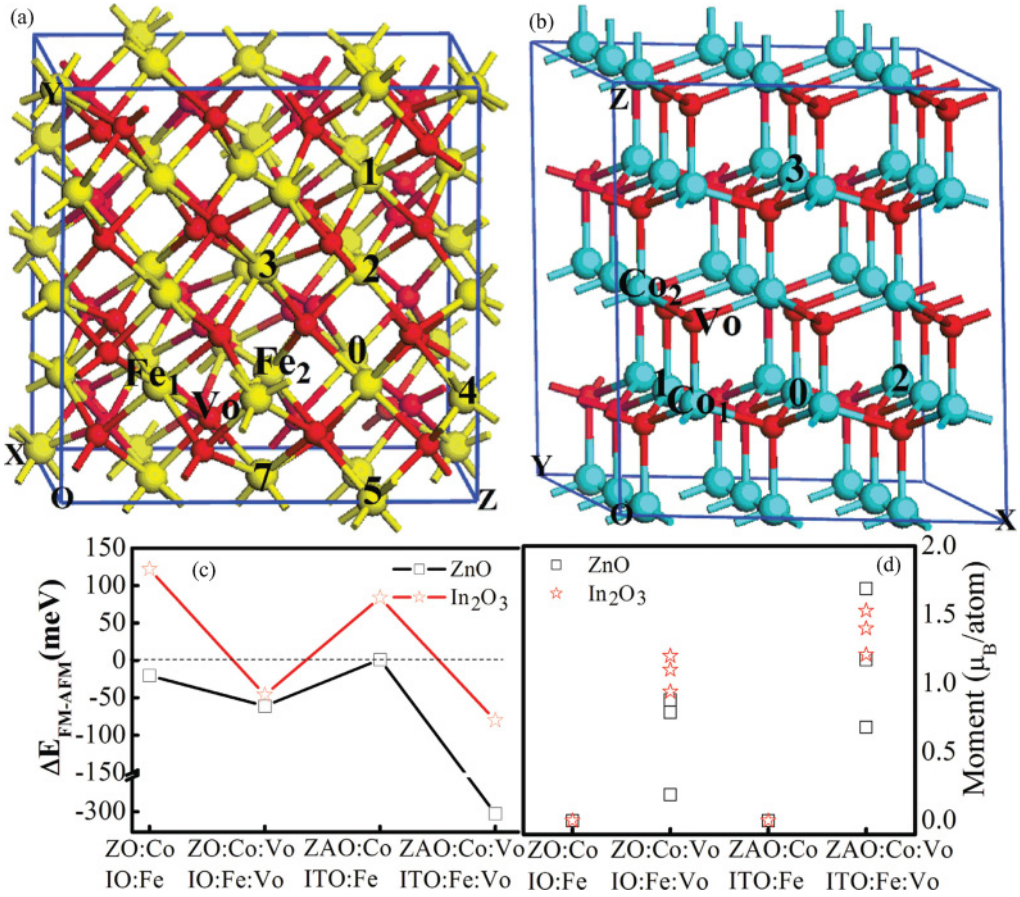

FIG. 1. (Color online) Supercells for (a) In_2O_3 and (b) ZnO. The yellow, blue, and red spheres represent In, Zn, and O atoms, respectively. In panel (a), the Sn atom is located at eight different configurations labeled by 0–7. In panel (b), the Al atom is located at four different configurations labeled by 0–3. Panel (c) provides the energy differences of the FM and AFM states in the most stable structures. Panel (d) provides the experimental data on RT magnetization.

total-energy calculations at the equilibrium volume. We have tested to ensure that these numerical parameters give sufficient accuracy and convergence. As representative tests, we have also used the GGA + U method to assess the importance of strong on-site correlations for some configurations. Our results show that the stability of the ferromagnetic (FM) state is quantitatively reduced relative to that of the antiferromagnetic (AFM) one, but on a qualitative level it does not alter our conclusions on the relative stability reached from the GGA calculations. As shown in Figs. 1(a) and 1(b), two extra Fe atoms or two extra Co are introduced into an 80 atom In_2O_3 cell or a 72 atom ($3 \times 3 \times 2$) ZnO cell, corresponding to 6.3% of Fe and 5.6% of Co, respectively, comparable to what was achieved in our experiments.

III. RESULTS AND DISCUSSIONS

We present the calculated results in the following order: evaluation of the equilibrium separation of two TM ions with and without an oxygen vacancy; the energies of the magnetic states of these configurations; the effect of adding free carriers in the absence of oxygen vacancy; and finally, the corporative effect of both oxygen vacancies and free carriers.

First, we discuss the energetically preferred structures of Fe-doped In_2O_3 and Co-doped ZnO. The GGA calculations for Fe-doped In_2O_3 indicate that the configuration consisting of two substitutional Fe atoms situated within a second nearest-neighbor (NN) distance is energetically the most favorable among all the calculated configurations. We denote this structure as IO:Fe. The two sites are indicated as Fe1 and Fe2 in Fig. 1(a). When an oxygen vacancy is also included, the most stable configuration is that where the bridging oxygen atom between the two Fe atoms is removed. We denote this configuration as IO:Fe:Vo. These structural results are in agreement with previous calculations.[31,32] In the Co-doped ZnO, we consider two configurations: the first Co atom is fixed at site Co1 and the second Co atom is placed at either the c NN (denoted as ZO:Co) or the b NN (denoted as ZO:Co^1) site, as shown in Fig. 1(b). The ZO:Co configuration is lower in total energy by only 2.8 meV than ZO:Co.[1] This difference is increased to 101.2 meV when a bridging oxygen vacancy, Vo, is introduced between the two Co atoms, resulting in a much more stable configuration of ZO:Co:Vo.

The magnetic energies of the stable structures described above for Fe-doped In_2O_3 and Co-doped ZnO with and without Vo are shown in Fig. 1(c); the energy differences ΔE between the ferromagnetic (FM) and antiferromagnetic (AFM) configurations of IO:Fe and IO:Fe:Vo in Fe-doped In_2O_3 are 121.9 and −46.2 meV, respectively. A negative value of ΔE implies that the FM state is more favorable, hence the

ground state of IO:Fe:Vo is ferromagnetic. For Co-doped ZnO, ZO:Co and ZO:Co[1] are −20.3 and 24.4 meV, respectively. These results indicate that the Co-Co interaction is FM along the *c* axis and AFM in the *a*-*b* plane. The addition of Vo makes the FM ordering of ZO:Co more stable, and ZO:Co:Vo becomes −61.0 meV. So far, these results confirm that Vo plays the important role of mediating the FM exchange coupling between two neighboring magnetic ions.[33]

Now we examine the effects of electron doping, first without the coexistence of Vo. The effects of electron doping in the absence of Vo is found by adding a Sn atom of valence +4 (2.1% Sn) to substitute a In^{3+} ion at sites 0–7 indicated in Fig. 1(a); the most stable configuration is denoted by ITO:Fe. For ZnO, an Al atom of valence +3 (2.8% Al) is added to replace a Zn^{2+} ion at sites 0–3 in Fig. 1(b) in ZO:Co; the most stable configuration is denoted by ZAO:Co. The energy differences between the FM and AFM states for ITO:Fe calculated for the eight configurations of Fe-Sn codoping in In_2O_3 are in the range from 73.6 to 87.2 meV, clearly favoring antiferromagnetism. Similarly, doping Al into ZO:Co without Vo destabilizes the FM ordering: for the four calculated configurations of Co/Al in ZnO, the energy differences are in the range from −10.4 to 1.25 meV, compared with the value of −20.3 meV for ZO:Co. Together, these results indicate that, without an oxygen vacancy, electron doping into Fe-doped In_2O_3 or Co-doped ZnO either favors AFM or weakens FM. This important finding is counterintuitive to the prevailing view of carrier-mediated magnetic ordering.[3,4]

Next we consider the effects of electron doping with the coexistence of Vo. We calculate the magnetic energies when we include Sn and Al in the most stable configurations of IO:Fe:Vo and ZO:Co:Vo identified earlier, as denoted by ITO:Fe:Vo and ZAO:Co:Vo, respectively. As shown in Fig. 1(c), the energy favoring ferromagnetic ordering is greatly enhanced in both cases. The largest magnitude occurring in ITO:Fe:Vo is −80 meV, further stabilizing the value of −46.2 meV for IO:Fe:Vo. Even more strikingly, the introduction of Al into ZO:Co:Vo decreases the value of ΔE from −61.3 meV to −324.3 meV in ZAO:Co:Vo. These results suggest a generic trend that carrier doping can enhance FM only in the presence of Vo.

Before proceeding any further on the theoretical investigations, here we present the preliminary experimental evidence supporting the above findings. In our experiments, high-purity In_2O_3 and ZnO powders together with their respective powdered Fe or Fe-Sn oxides and Co or Co-Al oxides were mixed, ground, and sintered in air for 12 h at 800 °C, yielding powders of 5% Fe or (5% Fe + 3% Sn) codoped In_2O_3 as well as 5% Co or (5% Co + 1−2% Al) codoped ZnO (this means atomic %). Using these powders as targets we obtain IO:Fe, ITO:Fe, ZO:Co, and ZAO:Co films deposited on Al_2O_3 (0001) substrates by pulse laser deposition (PLD). During the deposition, the substrate temperature was maintained at 600 °C and the O_2 pressure was less than 5×10^{-3} mTorr. The average film thickness is 100–200 nm. There are no second phases in the films detected by XRD: a plot is shown in Fig. 2. The IO:Fe and ITO:Fe films are mainly textured with (222) orientation, while the ZO:Co and ZAO:Co films are oriented with (002) plane. The corresponding magnetic moments of these samples are shown in Fig. 1(d). First, the Fe-doped In_2O_3 and Co-doped

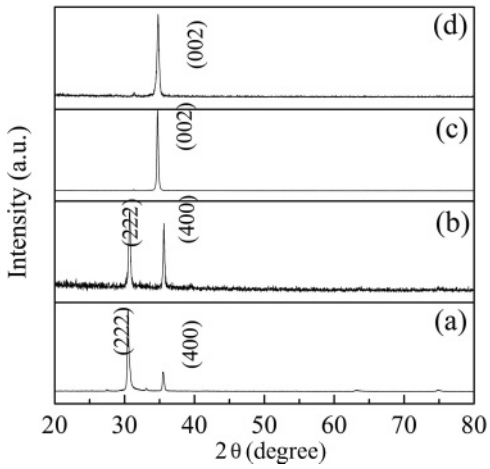

FIG. 2. The experimental XRD patterns of IO:Fe (a), ITO:Fe (b), ZO:Co (c), and ZAO:Co (d).

ZnO films with the range of carrier concentration $10^{19-20}/cm^3$ exhibit robust room-temperature ferromagnetism, but lose their magnetic ordering when they are annealed in air; due to eliminating the oxygen vacancies, the carrier concentrations of the air-annealed films have fallen to less than $10^{17}/cm^3$. The Fe-Sn or Co-Al codoped films again exhibit room-temperature ferromagnetism, and their carrier concentration is in the range of $10^{20-21}/cm^3$. Their average room-temperature (RT) magnetic moments are clearly enhanced from their counterparts of Fe or Co doped films. Finally, when annealed in air to remove the oxygen vacancies, these Fe-Sn or Co-Al codoped films again lose their ferromagnetism. This occurs even when the samples still show metallic conductivity with carrier density falling in the range of $10^{19-20}/cm^3$ due to the extrinsic donors. This contrasts with earlier studies without added extrinsic donors in which both the magnetism and the metallic conductivity vanished after annealing in air.[27,28] These experimental observations are in excellent qualitative agreement with the theoretical findings presented above.

Deeper understanding of the above theoretical and experimental observations requires a careful examination of the microscopic magnetic coupling mechanism within the systems. Figures 3(a) and 3(b) present the spin-density distribution around the oxygen vacancy in IO:Fe:Vo and ZO:Co:Vo. We find that the two Fe atoms in IO:Fe:Vo or the two Co atoms in ZO:Co:Vo are both in a spin-up state and coupled ferromagnetically through the spin-down electrons trapped by the oxygen vacancy, and form a local magnetic polaron.[15] For comparison, in Figs. 3(c) and 3(d) we plot the spin-density distribution around a TM dimer in ITO:Fe and ZAO:Co. In both cases, the TM dimer is antiferromagnetically coupled by the superexchange interaction via the bridging oxygen ion, as expected for wide-gap semiconductors.[34] Together, these results provide strong evidence that the bridging Vo is indispensable for inducing local ferromagnetism within the BMP. Another finding here is that the oxygen atoms around a BMP are spin polarized and have small moments. This is consistent with the observation by Martínez-Boubeta *et al.*, who found magnetic moments on oxygen atoms surrounding a Mg vacancy in a MgO film by the XMCD technique.[35] Here we also note that whether the TM ions are ferromagnetic is more

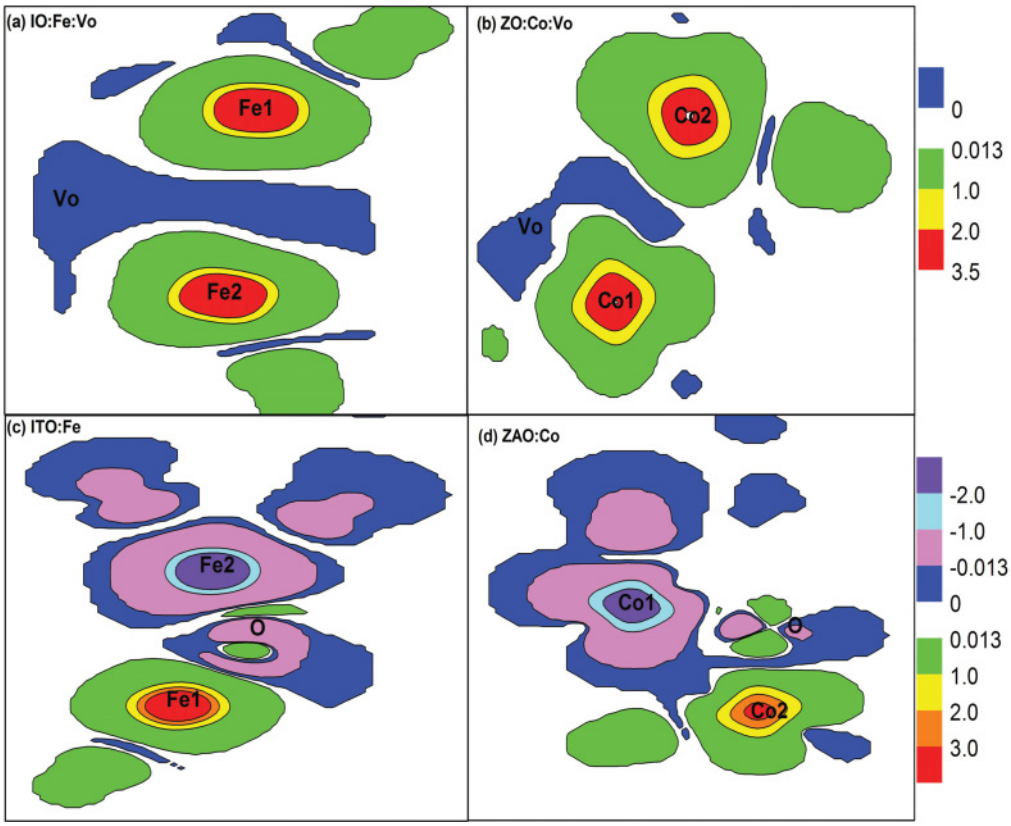

FIG. 3. (Color online) The spin density of (a) Fe-doped In_2O_3 and (b) Co-doped ZnO, both with oxygen vacancy. The bar on the right of panel (b) shows the color code of the magnetism in panels (a) and (b). Panels (c) and (d) correspond to the Fe-Sn codoped In_2O_3 and Co-Al codoped ZnO without oxygen vacancy. The corresponding color code of the magnetism is shown on the right of panel (d).

controversial; for example, some related studies using x-ray magnetic circular dichroism (XMCD) and Mössbauer spectroscopy found that the TM ions were nonmagnetic.[16,36] One possible explanation is that the binding energies of the 2TM-Vo complexes are large but not large enough to ensure a majority of the TM ions forming complexes at the growth temperature.[37] While this will not affect the global ferromagnetism and antiferromagnetism originating from those complexes, it may affect the results of the XMCD and Mössbauer spectroscopy measurements as these techniques tend to be more sensitive to the local behavior of the majority of TM ions. Future investigations may be required to clarify this important issue.

Figures 4(a)–4(d) present the density of states (DOS) spectra of ZO:Co:Vo and ZAO:Co:Vo with FM ordering. It is found that doping with Al causes a dramatic downward shift of the total DOS, and the Fermi level moves into the conduction band, resulting in the appearance of more mobile electrons, which are significant for producing FM in this system. As displayed in Figs. 4(c) and 4(d), a strong coupling exists between the $2p$ orbital of the oxygen atoms and the $3s$ orbital of the Al atom in ZAO:Co:Vo, making the FM state more stable than in ZO:Co:Vo. As displayed in Figs. 4(e)–4(h), similar coupling between the $2p$ orbitals of the oxygen atoms and the $4s$ orbital of the Sn atom also exists in ITO:Fe:Vo. It is noted that such an s-p coupling is stronger in ZAO:Co:Vo than that in ITO:Fe:Vo, explaining why ΔE for ZAO:Co:Vo is equal to -324.3 meV, much larger than -80.0 meV for ITO:Fe:Vo. These analyses confirm again that the electron doping can greatly enhance the FM stability of BMPs in Co-doped ZnO and Fe-doped In_2O_3.

We now turn to the other crucial role of electron doping, namely, the additional electrons can mediate the long-range FM coupling between the BMPs. We choose ZnO as an example and enlarge the supercell to $4 \times 3 \times 3$ and $6 \times 3 \times 2$ in order to consider two BMPs. As shown in Figs. 5(a) and 5(b), the distance between the BMPs is set at 4.61, 6.56, and 9.85 Å, respectively. In these cases, the two magnetic polarons are not as nearest neighbors. Figure 5(b) shows ΔE for Co-doped ZnO as a function of the BMP-BMP distance with and without Al doping. It is clear that, with Al doping, the values of ΔE are negative, decreasing in magnitude with the distance. At the distance of 9.85 Å, the concentration of Co atoms is 5.6%, much lower than the cation percolation threshold of 16.7% (calculated by $2/Z$, Z being the cation coordination of ZnO).[38] This indicates that the ferromagnetic exchange coupling between two BMPs is long range in Co-doped ZnO with electron doping. In contrast, no long-range FM (ΔE is positive) is obtained without Al doping for two BMPs separated by 4.61, 6.56, and 9.85 Å. These findings demonstrate that, besides enhancing the ferromagnetic stability of a BMP, electron doping is also essential to provide the nonlocal ferromagnetic coupling between the BMPs in oxide DMSs.

We all know that more defects will make the crystal quality worse, which is not good for practical devices. Actually, it is expected that additional carriers can control the transport

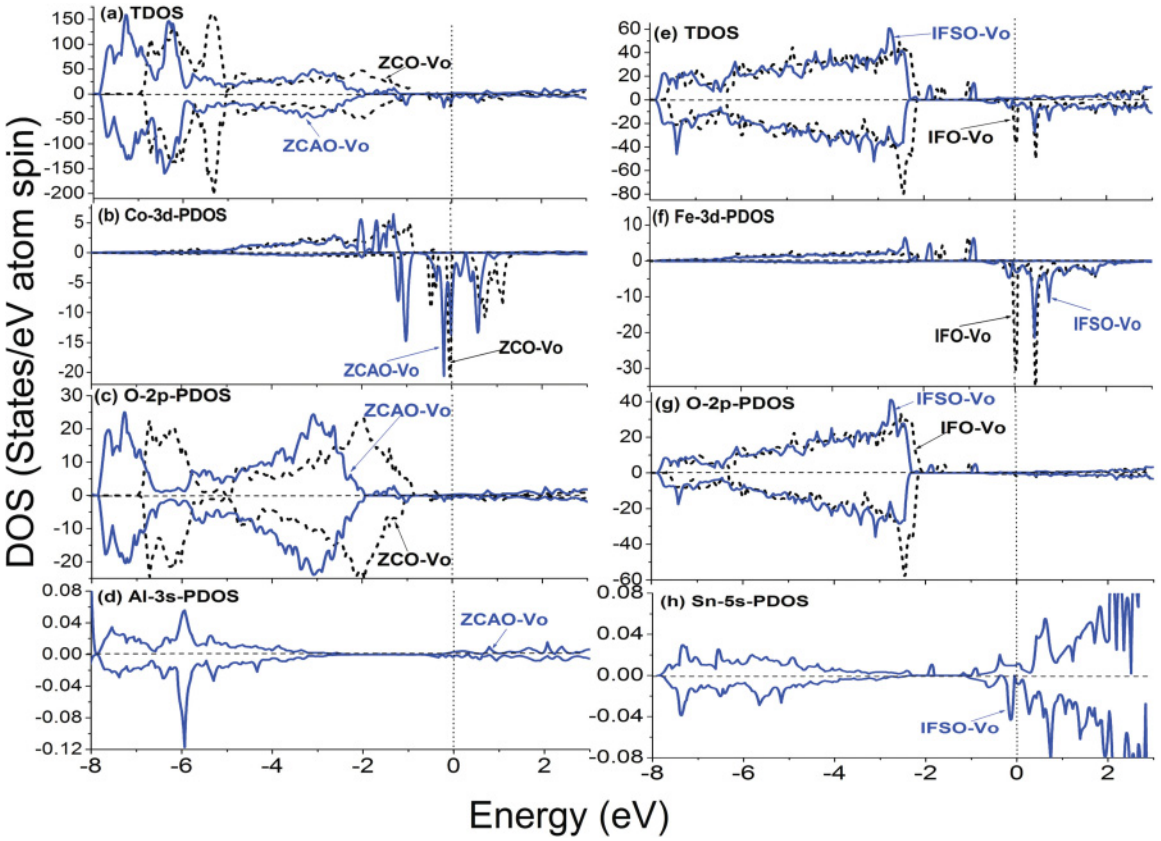

FIG. 4. (Color online) The total density of states (TDOSs) (a) and projected density of states (PDOSs) [(b)–(d)] of Co 3*d*, O 2*p*, and Al 3*s* for ZO:Co:Vo (dashed lines) and ZAO:Co:Vo. The TDOSs (e) and PDOSs [(f)–(h)] of Fe 3*d*, O 2*p*, and Sn 5*s* for IFO-Vo (dashed lines) and IFSO-Vo, respectively.

as well as magnetic properties in oxide DMSs. In this study, we find that the defect is necessary for producing the ferromagnetism, while electron doping plays the elegant dual role of further enhancing the ferromagnetic stability of a local polaron, and more crucially, mediating the nonlocal magnetic coupling of two polarons. Hence, we can draw the following conclusion on the origin of magnetism in oxide DMSs: a small quantity of oxygen vacancies is responsible for forming the bound magnetic polarons, and free carriers acting as an intermediary can help the long-range ferromagnetic coupling between the magnetic polarons. This explains the very large scatter of results reported in the literature. In addition, it also provides a guide for designing oxide-based spintronic devices.

IV. CONCLUSION

In summary, we have systematically studied the roles of oxygen vacancies and extrinsic carrier doping in mediating

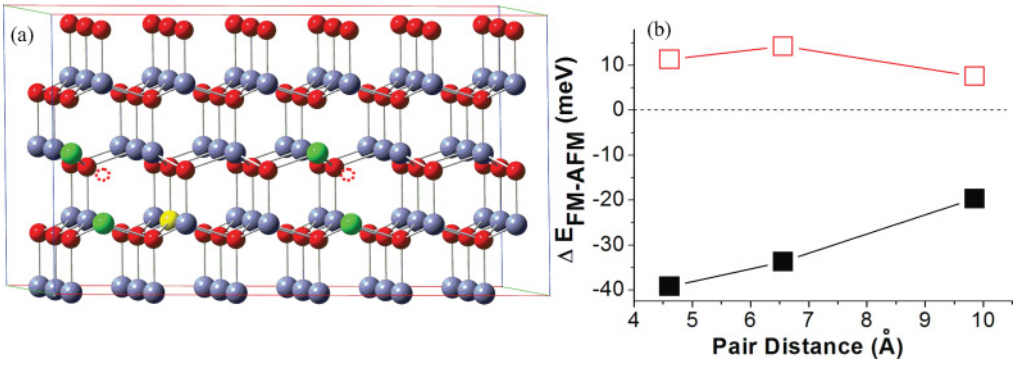

FIG. 5. (Color online) (a) The larger supercell of ZnO used to study the long-range ferromagnetic coupling of two BMPs. The gray and red spheres are Zn and O atoms, respectively, and the green and yellow spheres are Co and Al atoms, respectively. The dotted circles indicate oxygen vacancies. (b) The $\Delta E(\mathrm{FM} - \mathrm{AFM})$ of Co-doped ZnO as a function of the BMP-BMP separation. The filled and unfilled squares are the results with and without additional electron doping, respectively.

magnetic ordering in the prototype systems of Fe-doped In_2O_3 and Co-doped ZnO by first-principles calculations and experiment. These studies led us to draw the following physical picture on ferromagnetic ordering in oxide DMSs: The oxygen vacancies are indispensable for stabilizing local ferromagnetism in the form of bound magnetic polarons; furthermore, carrier doping plays the dual role of further enhancing the ferromagnetic stability of local polarons and also mediating the nonlocal magnetic coupling between two magnetic polarons.

ACKNOWLEDGMENTS

This work was supported in part by the NSFC for Distinguished Young Scholars (Grant No. 51025101), the 863 Program (Grant No. 2009AA03Z446), the NSFC (Grant Nos. 10574085, 0776008, 11034006, and 11104173), NCET-07-0527, and in part by the Division of Materials Science and Engineering, Office of Basic Energy Sciences, US Department of Energy, and USNSF (Grant No. 0906025). S.B.Z. is supported by the US Department of Energy under Grant No. DE-SC0002623.

*Corresponding author: xuxh@dns.sxnu.edu.cn

[1] T. Dietl, H. Ohno, F. Matsukura, J. Cibert, and D. Ferrand, Science **287**, 1019 (2000).
[2] S. A. Wolf, D. D. Awschalom, R. A. Buhrman, J. M. Daughton, S. von Molnár, M. L. Roukes, A. Y. Chtchelkanova, and D. M. Treger, Science **294**, 1488 (2001).
[3] I. Zutic, J. Fabian, and S. Das Sarma, Rev. Mod. Phys. **76**, 323 (2004).
[4] T. Jungwirth, J. Sinova, J. Masek, J. Kucera, and A. H. MacDonld, Rev. Mod. Phys. **78**, 809 (2006).
[5] H. Ohno, Science **281**, 951 (1998).
[6] Y. D. Park, A. T. Hanbicki, S. C. Erwin, C. S. Hellberg, J. M. Sullivan, J. E. Mattson,T. F. Ambrose, A. Wilson, G. Spanos, and B. T. Jonker, Science **295**, 651 (2001).
[7] Y. Matsumoto, M. Murakami, T. Shono, T. Hasegawa, T. Fukumura, M. Kawasaki, P. Ahmet, T. Chikyow, S. Koshihara, and H. Koinuma, Science **291**, 854 (2001).
[8] J. Philip, A. Punnoose, B. I. Kim, K. M. Reddy, S. Layne, J. O. Holmes, B. Satpati, P. R. Leclair, T. S. Santos, and J. S. Moodera, Nat. Mater. **5**, 298 (2006).
[9] S. B. Ogale, R. J. Choudhary, J. P. Buban, S. E. Lofland, S. R. Shinde, S. N. Kale, V. N. Kulkarni, J. Higgins, C. Lanci, J. R. Simpson, N. D. Browning, S. Das Sarma, H. D. Drew, R. L. Greene, and T. Venkatesan, Phys. Rev. Lett. **91**, 077205 (2003).
[10] F. Pan, C. Song, X. J. Liu, Y. C. Yang, and F. Zeng, Mater. Sci. Eng. R **62**, 1 (2008).
[11] A. Walsh, J. L. F. Da Silva, and S. H. Wei, Phys. Rev. Lett. **100**, 256401 (2008).
[12] K. Sato and H. K. Yoshida, Jpn. J. Appl. Phys. **40**, L334 (2001).
[13] M. Ruderman and C. Kittel, Phys. Rev. **96**, 99 (1954).
[14] D. M. Edwards and M. I. Katsnelson, J. Phys.: Condens. Matter. **18**, 7209 (2006).
[15] J. M. D. Coey, M. Venkatesan, and C. B. Fitzgerald, Nat. Mater. **4**, 173 (2005).
[16] J. M. D. Coey, P. Stamenov, R. D. Gunning, M. Venkatesan, and K. Paul, New J. Phys. **12**, 053025(2010).
[17] M. H. F. Sluiter, Y. Kawazoe, P. Sharma, A. Inoue, A. R. Raju, C. Rout, and U. V. Waghmare, Phys. Rev. Lett. **94**, 187204 (2005).
[18] H. S. Hsu, J. C. A. Huang, Y. H. Huang, Y. F. Liao, M. Z. Lin, C. H. Lee, J. F. Lee, S. F. Chen, L. Y. Lai, and C. P. Liu, Appl. Phys. Lett. **88**, 242507 (2006).
[19] S. C. Li, P. Ren, B. C. Zhao, B. Xia, and L. Wang, Appl. Phys. Lett. **95**, 102101 (2009).
[20] T. Matsumura, D. Okuyama, S. Niioka, H. Ishida, T. Satoh, Y. Murakami, H. Toyosaki, Y. Yamada, T. Fukumura, and M. Kawasaki, Phys. Rev. B **76**, 115320 (2007).
[21] X. H. Xu, H. J. Blythe, M. Ziese1, A. J. Behan, J. R. Neal, A. Mokhtari, R. M. Ibrahim, A. M. Fox, and G. A. Gehring, New J. Phys. **8**, 135 (2006).
[22] A. J. Behan, A. Mokhtari, H. J. Blythe, D. Score, X.-H. Xu, J. R. Neal, A. M. Fox, and G. A. Gehring, Phys. Rev. Lett. **100**, 047206 (2008).
[23] D. Mukherjee, T. Dhakal, H. Srikanth, P. Mukherjee, and S. Witanachchi, Phys. Rev. B **81**, 205202 (2010).
[24] H. Raebiger, S. Lany, and A. Zunger, Phys. Rev. Lett. **101**, 027203 (2008).
[25] J. Alaria, N. Cheval, K. Rode, M. Venkatesan, and J. M. D. Coey, J. Phys. D: Appl. Phys. **41**, 135004 (2008).
[26] J. M. D. Coey, P. Stamenov, R. D. Gunning, M. Venkatesan, and K. Paul, New J. Phys. **12**, 053025 (2010).
[27] K. R. Kittlstved, N. S. Norberg, and D. R. Gamelin, Phys. Rev. Lett. **94**, 147209 (2005).
[28] N. Khare, M. J. Kappers, M. Wei, M. G. Blamire, and J. L. MacManus-Driscoll, Adv. Mater. **18**, 1449 (2006).
[29] P. E. Blöchl, Phys. Rev. B **50**, 17953 (1994).
[30] G. Kresse and J. Furthmuller, Phys. Rev. B **54**, 11169 (1996).
[31] L. X. Guan, J. G. Tao, Z. R. Xiao, B. C. Zhao, X. F. Fan, C. H. A. Huan, J. L. Kuo, and L. Wang, Phys. Rev. B **79**, 184412 (2009).
[32] S. Hu, S. Yan, X. Lin, X. Yao, Y. Chen, G. Liu, and L. Mei, Appl. Phys. Lett. **91**, 262514 (2007).
[33] C. D. Pemmaraju, R. Hanafin, T. Archer, H. B. Braun, and S. Sanvito, Phys. Rev. B **78**, 054428 (2008).
[34] K. Sato, L. Bergqvist, J. Kudrnovsky, P. H. Dederichs, O. Eriksson, I. Turek, B. Sanyal, G. Bouzerar, H. Katayama-Yoshida, V. A. Dinh, F. Fukushima, H. Kizaki, and R. Zeller, Rev. Mod. Phys. **82**, 1634 (2010).
[35] C. Martínez-Boubeta, J. I. Beltrán, L. Balcells, Z. Konstantinovic, S. Valencia, D. Schmitz, J. Arbiol, S. Estrade, J. Cornil, and B. Martínez, Phys. Rev. B **82**, 024405 (2010).
[36] T. Tietze, M. Gacic, G. Schütz, G. Jakob, S. Brück, and E. Goering, New J. Phys. **10**, 055009 (2008).
[37] T.-L. Chan, D. West, and S. B. Zhang, Phys. Rev. Lett. **107**, 035503 (2011).
[38] *Percolation Structures and Processes*, edited by G. Deutscher, R. Zallen, and J. Adler (Adam Hilger, Bristol, 1983).